The Astrophysical Journal, 599:1049–1066, 2003 December 20

THE MASS FUNCTION OF SUPERGIANT MOLECULAR COMPLEXES AND IMPLICATIONS FOR FORMING YOUNG MASSIVE STAR CLUSTERS IN THE ANTENNAE (NGC 4038/4039)

Christine D. Wilson,[1] Nicholas Scoville,[2] Suzanne C. Madden,[3] and Vassilis Charmandaris[4]
Received 2002 October 22; accepted 2003 August 29

ABSTRACT

We have used previously published observations of the CO emission from the Antennae (NGC 4038/4039) to study the detailed properties of the supergiant molecular complexes with the goal of understanding the formation of young massive star clusters. Over a mass range from 5×10^6 to 9×10^8 $M_\odot$ the molecular complexes follow a power-law mass function with a slope of -1.4 ± 0.1, which is very similar to the slope seen at lower masses in molecular clouds and cloud cores in the Galaxy. Compared with the spiral galaxy M51, which has a similar surface density and total mass of molecular gas, the Antennae contain clouds that are an order of magnitude more massive. Many of the youngest star clusters lie in the gas-rich overlap region, where extinctions as high as $A_V \sim 100$ mag imply that the clusters must lie in front of the gas. Young clusters found in other regions of the galaxies can be as far as 2 kpc from the nearest massive cloud, which suggests that either young clusters can form occasionally in clouds less massive than 5×10^6 $M_\odot$ or that these young clusters have already destroyed their parent molecular clouds. Combining data on the young clusters, thermal and nonthermal radio sources, and the molecular gas suggests that young massive clusters could have formed at a constant rate in the Antennae over the last 160 Myr and that sufficient gas exists to sustain this cluster formation rate well into the future. However, this conclusion requires that a very high fraction of the massive clusters that form initially in the Antennae do not survive as long as 100 Myr. Furthermore, if most young massive clusters do survive for long periods, the Antennae must be experiencing a relatively short burst of cluster formation to prevent the final merger remnant from exceeding the observed specific frequency of star clusters in elliptical galaxies by a wide margin. Finally, we compare our data with two models for massive star cluster formation and conclude that the model in which young massive star clusters form from dense cores within the observed supergiant molecular complexes is most consistent with our current understanding of this merging system.

Subject headings: galaxies: individual (NGC 4038, NGC 4039) — galaxies: ISM — ISM: molecules — radio lines: galaxies — stars: formation

1. INTRODUCTION

The discovery of very luminous young star clusters in merger remnant galaxies (Holtzman et al. 1992; Whitmore et al. 1993; Whitmore & Schweizer 1995) has led to a dramatic shift in our understanding of star cluster formation. Some of these young star clusters may be massive enough (Zhang & Fall 1999; Ho & Filippenko 1996; Mengel et al. 2002) that they can be viewed as young counterparts to the ubiquitous globular clusters, which are found in nearly every extragalactic system from giant cD elliptical galaxies to dwarf irregular galaxies (Harris 2001). The discovery of these young massive clusters suggests that massive star cluster formation was not a process confined exclusively to the early universe (e.g., Cen 2001; Fall & Rees 1985) but rather one that continues to the present day. Thus, while attempting to understand the formation and evolution of young massive star clusters is interesting in its own right, such studies may also shed light on the process of globular cluster formation, which clearly occurred in a wide variety of galactic environments in the early universe.

Since star clusters in the Milky Way are observed to form in dense clouds of molecular hydrogen gas, it is likely that these young massive star clusters formed in a similar way. However, the relatively large masses ($>10^5$ $M_\odot$) estimated for these clusters are comparable to the masses of typical giant molecular clouds in nearby galaxies (Sanders, Scoville, & Solomon 1985). Since individual molecular clouds typically form stars with efficiencies of only a few percent (Evans & Lada 1991), these large cluster masses pose a challenge to our current understanding of star formation. In particular, if the star clusters are gravitationally bound, the star formation efficiency in the material from which they formed must have been closer to 50%. Such high star formation efficiency is typically observed only in smaller bound cores within individual giant molecular clouds (Lada et al. 1991b). These facts have led to two quite different explanations for how these young massive star clusters formed. To explain the formation of globular clusters, Harris & Pudritz (1994) postulated the existence of "supergiant molecular clouds" in the early universe. With masses up to 10^9 $M_\odot$ but internal structures similar to local giant molecular clouds, these massive clouds could contain correspondingly massive cores, which could form massive (bound) star clusters. If similarly massive clouds exist in galaxies in the local universe, this might also be a viable method for forming young massive star clusters. An alternative explanation for young massive

[1] Department of Physics and Astronomy, McMaster University, Hamilton, ON L8S 4M1, Canada; wilson@physics.mcmaster.ca.
[2] Division of Physics, Mathematics, and Astronomy, MS 105-24, California Institute of Technology, Pasadena, CA 91125.
[3] Commissart à L'Energie Atomique/DSM/DAPNIA/Service d'Astrophysique, CE-Saclay, 91191 Gif-sur-Yvette Cedex, France.
[4] Department of Astronomy, Cornell University, 610 Space Sciences Building, Ithaca, NY 14853-6801; Chercheur Associé, Observatoire de Paris, LERMA, 61 Avenue de l'Observatoire, F-75014 Paris, France.

star clusters proposed by Schweizer et al. (1996) involves the collapse of a preexisting giant molecular cloud to form a single massive star cluster. Such collapse could be triggered by overpressure in the diffuse interstellar medium produced during the collision of two massive galaxies (Jog & Solomon 1992) but would require a collapse of 2–3 orders of magnitude in linear size. Clearly, one way to shed some light on the processes that lead to the formation of young massive star clusters is to study the properties of the molecular gas in galaxies in which such clusters are found.

Since the original discoveries of rich populations of young massive star clusters in nearby merging and merger remnant galaxies, young massive clusters have been identified in a very wide range of galactic environments, from dwarf starburst galaxies (e.g., M82; O'Connell et al. 1995) to spiral galaxies (e.g., M51; Larsen 2000) to merging galaxies in all stages of evolution (see Whitmore 2003 for a complete list). The Antennae system (NGC 4038/4039= Arp 244) has the largest number of young massive star clusters identified in a single galaxy to date (Whitmore & Schweizer 1995; Whitmore et al. 1999). In addition, the clusters in the Antennae are spread over a large area of the galaxy ($\sim$100 kpc^2), which implies that these clusters have formed over much of the galactic disks. The Antennae have a higher surface density of young massive star clusters than older merger systems, although smaller galaxies such as M82 (O'Connell et al. 1995) have a larger absolute surface density of clusters confined to a relatively small region. This extremely rich population of clusters, combined with the proximity of the Antennae system (19 Mpc for $H_0 = 75$ km s^{-1} Mpc^{-1}), makes it the logical first choice for detailed studies of the structure and properties of the molecular interstellar medium with the aim of understanding the formation of young massive star clusters.

The first detection of CO in the Antennae, by Sanders & Mirabel (1985), suggested that the system had a relatively high ratio of far-infrared to CO luminosity. More recent complete mapping of the two galactic disks by Gao et al. (2001) revealed a much larger reservoir of molecular gas, which led to the suggestion that this system could possibly evolve into an ultraluminous starburst as the merging becomes more advanced. Early interferometric CO observations of the Antennae system were presented by Stanford et al. (1990). These observations revealed that the most massive concentration of molecular gas lay outside the two nuclei in a region that Stanford et al. named "the overlap region." In a recent paper (Wilson et al. 2000, hereafter Paper I), we presented interferometric CO observations of the Antennae with improved resolution and sensitivity and covering a larger fraction of the galactic disks. These data show the presence of massive ($>10^8$ $M_\odot$) gravitationally bound gas clouds, which we term "supergiant molecular complexes" (Paper I). A detailed comparison of the CO data with high-resolution mid-infrared data from the *Infrared Astronomical Satellite* (Vigroux et al. 1996; Mirabel et al. 1998) suggests that the extremely bright mid-infrared source seen in the overlap region could be produced by star formation induced by the collision of two of these massive complexes (however, see Liang et al. 2001 for evidence that the clouds may not be colliding). An alternative explanation is that this region contains extremely young ($<$1 Myr) sites of star formation (Paper I).

In this paper, we use the data set presented in Paper I for a detailed study of the population of molecular complexes in the Antennae, such as their mass function, their spatial overlap with the young massive star clusters, and a comparison with theories of star cluster formation. In § 2 we describe the observations and data reduction, as well as briefly discuss how the clouds were identified from the data cube. In § 3 we present the cloud mass spectrum and compare our results with observations of massive cloud complexes in other nearby galaxies. We also discuss what can be learned from the relative locations of the young massive star clusters and the supergiant molecular complexes. In § 4, we make a detailed comparison of the Antennae with the complexes and star clusters observed in M51 (Rand & Kulkarni 1990; Larsen 2000; Scoville et al. 2001). In § 5 we discuss the recent star formation history in the Antennae, and in § 6 we compare the properties of the molecular complexes with two models for massive star cluster formation. The paper is summarized in § 7.

2. ANALYSIS

2.1. *Observations and Data Reduction*

The CO observations of the Antennae originally presented in Paper I were obtained with the Caltech Millimeter Array between 1998 March and 1999 February. Three overlapping field centers were chosen to cover the majority of the young massive star clusters identified by Whitmore & Schweizer (1995). The coordinates of the three field centers were specified in 1950 coordinates as ($11^h59^m20^s.3$, $-18°35'31''$) (field 1), ($11^h59^m20^s.3$, $-18°36'11''$) (field 2), and ($11^h59^m17^s.5$, $-18°35'21''$) (field 3), which gives an offset between adjacent field centers of $40''$. In J2000.0 coordinates, the equivalent field centers are ($12^h01^m54^s.09$, $-18°52'13''.25$), ($12^h01^m54^s.09$, $-18°52'53''.25$), and ($12^h01^m51^s.28$, $-18°52'03''.25$), respectively. Each field was observed for the equivalent of one complete transit in each of four configurations: C (compact), L (low), E (equatorial), and H (high resolution). The baselines for these observations ranged from 15 to 250 m. The observations of Fields 1 and 2 were interleaved in each observing track, which results in very similar *u-v* coverage for these two fields. Field 3 (which was added later) was observed in separate tracks. These CO data represent approximately 90 hr observing time with the array.

The spectrometer was configured to give 2 MHz (5.2 km s^{-1}) resolution and was tuned to a central velocity of 1547 km s^{-1}; the resulting velocity range was from 1256 to 1838 km s^{-1}. The system temperatures obtained during these observations range from 1000 to 2000 K (single sideband), with an average value of 1500 K. (Note that these system temperatures are substantially higher than those typically obtained by the array because of the low declination of the source.) The data calibration was performed using the MMA package (Scoville et al. 1993). The bright quasar 3C 273 was observed for flux calibration; its flux was derived from observations of either Uranus or Neptune taken from other observing sessions in the array database. The flux of 3C 273 changed slowly during the 12 months over which these data were obtained. The following values were derived for the flux of 3C 273: 21 Jy (1998 March–May), 22 Jy (1998 September–November 1), 19.5 Jy (1998 November 1–December 20), and 17 Jy (1998 December 20–1999 February 16). The absolute calibration uncertainty is estimated to be 20%. The gain and passband calibrator for these observations was the bright quasar 3C 279. Only observations for

which the coherence on 3C 279 was measured to be greater than 50% were included in the final analysis.

The data were mapped using the MIRIAD analysis package (Sault, Teuben, & Wright 1995). The *u-v* data were first clipped to have a maximum amplitude of 14 Jy. The three fields were inverted together with robust weighting to make a single mosaic dirty map. The rms noise in this dirty map in line-free channels was 0.055 Jy beam^{-1}, and the synthesized beam was $3''.15 \times 4''.91$ (or 310×480 pc at a distance of 19 Mpc). The map was cleaned using the task MOSSDI with a clean cutoff of 0.11 Jy beam^{-1} (2 σ). We used a single clean box made by summing three $60'' \times 60''$ clean boxes centered on each of the three field centers. As a final step, individual maps and the data cube were corrected for the falloff in sensitivity due to the primary beam of the 10.4 m antennas. We used the task MOSSEN to create a map of the gain due to the primary beam and then divided individual maps by that gain file, while also masking regions of the maps where the gain map was smaller than 0.5.

2.2. *Identifying Clouds from the Data Cube*

Individual clouds were identified from the data cube by using the automatic clump identification algorithm CLFIND (Williams, de Geus, & Blitz 1994). This algorithm searches for peaks of emission within a contour map of the data, which it then follows down to lower intensity levels, and has the advantage of not assuming any specific clump profile (such as a Gaussian profile). The main free parameter in the algorithm is the contour level, which defines our cloud detection threshold. The contour level is specified relative to the noise in the map and is usually set to 2 σ. Only emission brighter than one contour level can be included in a cloud, and a cloud must have at least 1 pixel that is twice the minimum contour level to be found. Thus, the initial cloud identification was run on the data cube before correction for primary beam attenuation. We experimented with three different contour levels to see how the contour level affected the properties of the clouds; we used contour levels of 0.10, 0.11 (2 σ), and 0.12 Jy beam^{-1}. Unlike in Paper I, individual clouds were not inspected and merged by hand where they appeared to overlap; thus, the properties of the largest clouds are somewhat different from the values in Paper I.

The properties of the individual clouds such as position, flux, and velocity were measured using the program CLSTATS (Williams et al. 1994). This program combines the clump assignment cube produced by CLFIND with the original data cube to calculate the parameters of the individual clouds from the pixels that have been assigned to that cloud. We used the gain-corrected data cube in running CLSTATS to produce fluxes that were corrected for the primary beam. The properties of the clouds measured with a contour level of 0.11 Jy beam^{-1} are given in Appendix A.

To estimate the sensitivity of the flux of an individual cloud (and hence its mass) to the chosen contour level, we took a closer look at the largest clouds in our sample, those with masses estimated to be larger than 10^8 $M_\odot$. Nine large clouds identified with a contour level of 0.11 Jy beam^{-1} were cross-identified with the lists from the other two contour levels, and the masses measured for each of the three identification runs were compared. The average dispersion in the mass measurements determined from the three different identification runs was 25%, while the dispersion for an individual cloud ranged from a low of 0% to a high of 55%. Thus, we estimate the random uncertainty on the mass estimate for any individual cloud in our sample to be 25%.

2.3. *Moment Maps and Total Flux*

The integrated intensity map presented in Paper I was made using the command CLPLOT to sum together the emission in the data cube that corresponded to molecular complexes identified by CLFIND. Only molecular complexes with emission in at least three velocity channels were included in the integrated intensity map. Thus, this image (shown again in Fig. 1*a*) differs from a standard zeroth-moment map because very small clouds and isolated weak emission regions have not been included.[5] An integrated intensity map (not shown) produced in the same way but including *all* the complexes identified by CLFIND, no matter how weak, is very similar to the positive contours in the zeroth-moment map made with a 2 σ intensity cutoff (Fig. 1*c*). Figure 2 shows the first-moment map of the molecular complexes in the Antennae. The original data cube was filtered by keeping only emission that CLFIND identified with a molecular complex; the first-moment map was produced from this filtered data cube with no additional flux cutoff. Thus, this first-moment map includes emission down to a level of 2 σ but is somewhat cleaner than a first-moment map made with a 2 σ cutoff from the original data cube because isolated emission regions extending over fewer than 4 pixels have not been included.

The zeroth-moment map shows clear negative bowls (which are not shown in Fig. 1 for clarity) around the bright emission regions, which are a sign that we are not detecting all the flux in the region with the interferometer. These negative bowls make it difficult to measure the total flux, so the total flux was measured instead from the integrated intensity image from CLPLOT, which included the very small clouds. The integrated intensity measured in this way is 930 Jy km s^{-1}, compared with 910 Jy km s^{-1} measured in Paper I. This flux is probably a slight underestimate of the total flux in the map, since CLFIND sometimes misses weak emission at the edges of clouds. To correct for this effect, we calculated the difference between the CLFIND map and the zeroth-moment map and measured an additional flux of 125 Jy km s^{-1} in the two nuclei and the overlap region where significant positive signal was seen. Thus, the final estimate of the total integrated intensity detected with the interferometer is 1055 Jy km s^{-1}. By adopting a CO-to-H_2 conversion factor of 3×10^{20} H_2 cm^{-2} (K km s^{-1})$^{-1}$ (Strong et al. 1988) and including a factor of 1.36 to account for heavy elements, this intensity corresponds to 6.1×10^9 $M_\odot$ of molecular gas. In Appendix B, we estimate the CO-to-H_2 conversion factor for the Antennae from a few large clouds and find that it agrees with the Galactic value within the uncertainties.

Gao et al. (2001) have made a complete single-dish map of the Antennae system. They measure a total flux of 3172 Jy km s^{-1}, which, for the same distance and conversion factor adopted above, corresponds to a total mass of 1.8×10^{10} $M_\odot$. This flux is significantly larger than the flux

[5] The version of CLPLOT that was used in this analysis had a bug in that the last cloud of a list of 20 was not included in the plots. This bug resulted in one small cloud not being included near the southern end of the west ring and some small changes to the contours around the two nuclei. The corrected version of the plot is shown in Fig. 1*b*.

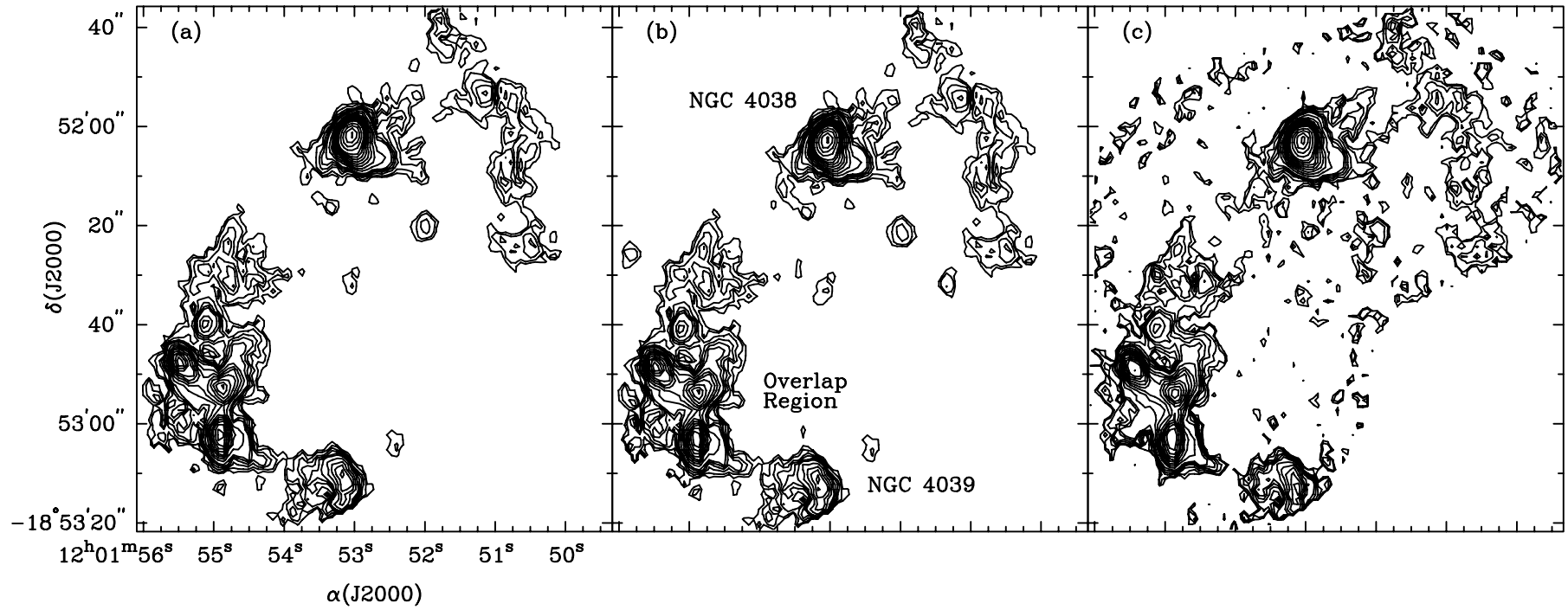

FIG. 1.—(*a*) Integrated CO intensity map from Paper I. Contour levels are 1, 2, 4, 6, 8, 10, 15, 20, 25, . . . , 50, 60, . . . , 90 Jy beam^{-1} km s^{-1}. This map was made using CLPLOT and including only molecular complexes with velocity widths greater than or equal to 15.6 km s^{-1} found with CLFIND. This image has been corrected for the falloff in sensitivity due to the primary beam. (*b*) Integrated intensity map made using the same data set and criteria but including the clouds that were missed because of a bug in the CLFIND program. (*c*) Standard zeroth-moment map made from the same data cube used to identify molecular complexes. The 50% gain limit of the telescope primary beam is clearly visible in this figure. Negative bowls exist in this map (see text) but are not shown for ease of comparison with the other two maps.

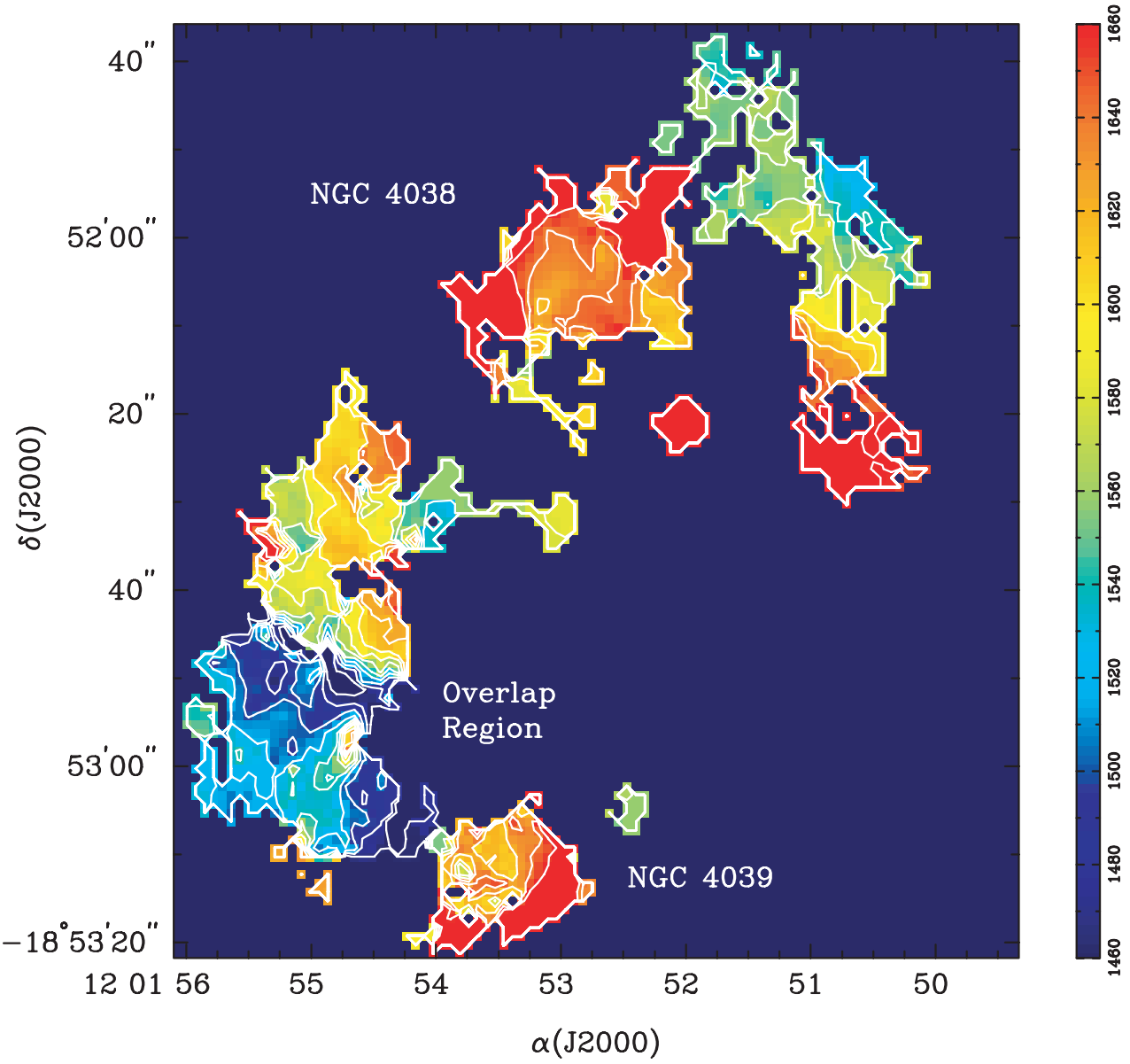

FIG. 2.—First-moment map of the CO emission in the Antennae. The color scale runs from 1460 to 1660 km s^{-1}, while the contour levels run from 1460 to 1660 km s^{-1} in steps of 20 km s^{-1}. Note in particular the disturbed velocity field in the overlap region.

detected in our interferometric map. However, their map, which contains 73 spectra at 28″ spacing, covers a substantially larger area than does our map. To estimate the single-dish flux within our smaller map, we summed the spectral lines from 14 spectra that fell within the clean box used in processing the interferometer map. The total flux from these 14 spectra is 1654 Jy km s^{-1} for a mass of 9.6×10^9 $M_\odot$. Thus, the interferometer map appears to have detected 65% of the total flux seen over the same area in the fully sampled single-dish map.

3. MOLECULAR COMPLEXES IN THE ANTENNAE AND OTHER GALAXIES

3.1. *Mass Spectrum of the Molecular Complexes*

We measured the mass spectrum for the molecular complexes in the Antennae by using the three different contouring levels discussed in § 2 to see whether the slope and upper mass cutoff to the mass spectrum were heavily dependent on the contour used to identify the clouds. The total number of complexes identified was 114 for a contour level of 0.10 Jy beam^{-1}, 86 for a contour level of 0.11 Jy beam^{-1}, and 49 for a contour level of 0.12 Jy beam^{-1}. For each set of complexes, we calculated the number of the clouds in logarithmic mass bins with a spacing of 0.2; two different centers for the mass bins were also used, with the first having a bin centered at $\log M = 7.0$ and the second having a bin centered at $\log M = 7.1$. The number of clouds in each mass bin was then divided by the central mass of that bin to obtain a true differential mass function, dN/dM. The differential mass functions for the three different identification runs are shown in Figure 3.

We calculated the detection and completeness limits for our data by using a modified version of the formulae given in Heyer, Carpenter, & Snell (2001). For these

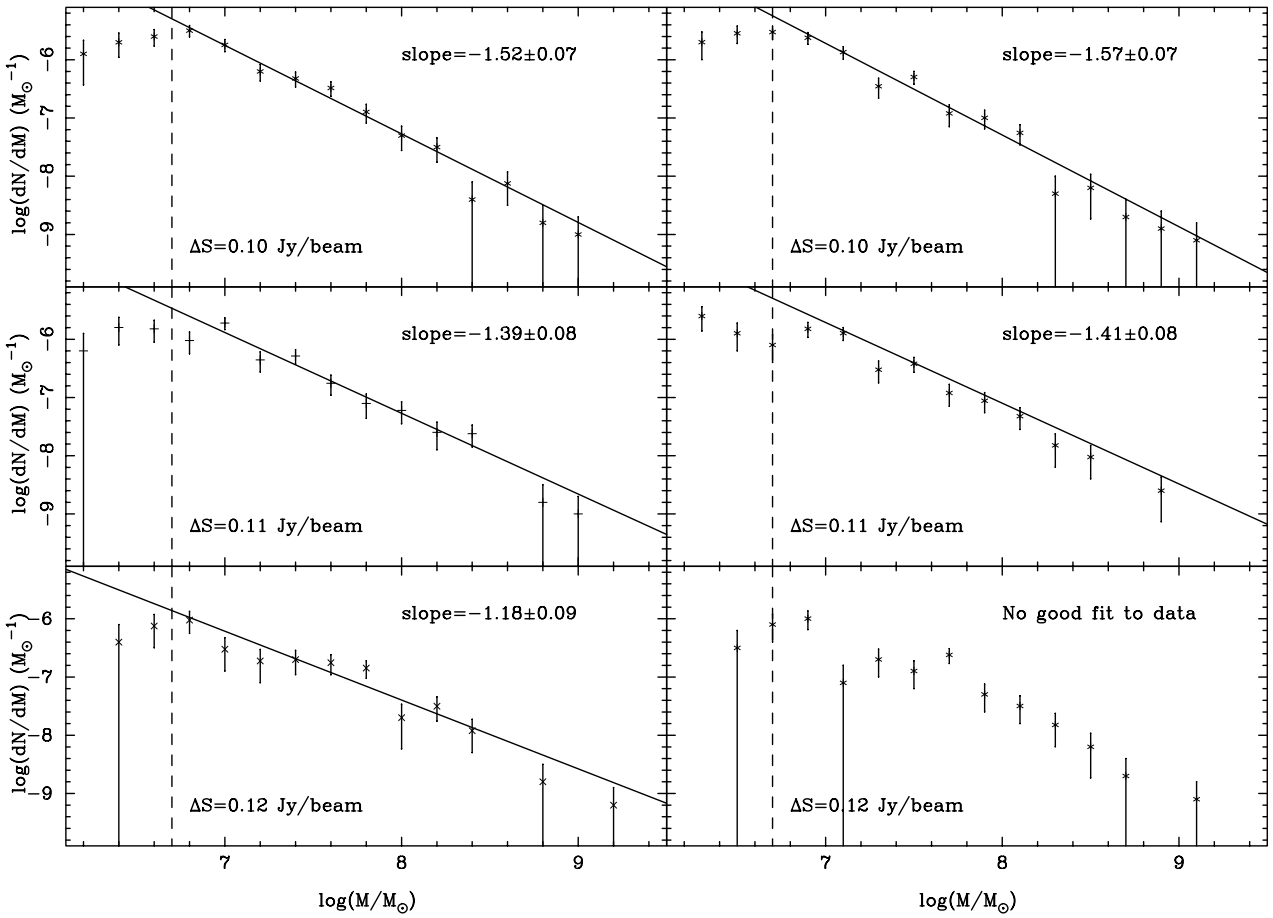

FIG. 3.—Differential mass function for the molecular complexes in the Antennae. Mass functions are shown for three identification runs with different contour levels; each identification run is also shown for two different binnings of the mass function separated by 0.1 in $\log M$. The 5 σ completeness limit is indicated by the dashed line. The contour level in Jy beam^{-1} and the slope derived from a least-squares fit to the points above the completeness limit are given in each plot. The average slope of -1.4 ± 0.1 is very similar to the slope observed for giant molecular clouds (10^3–10^6 $M_\odot$) in the Milky Way.

interferometric data processed using CLFIND, a cloud must contain at least 4 pixels, 1 of which exceeds twice the specified contour level, to be detected. The detection limit in Jy km s^{-1} is then given by

$$S_{\rm CO}^{\rm min} = 5\Delta S \Delta V / 17.55 \, ,$$

where ΔS is the contour level in janksys per beam, ΔV is the velocity width of a single channel (5.2 km s^{-1}), and the factor of 17.55 is the area of the synthesized beam in pixels. For $\Delta S = 0.11$ Jy beam^{-1}, the detection limit is $S_{\rm CO}^{\rm min} = 0.16$ Jy km s^{-1}. The 5 σ completeness limit is given by

$$S_{\rm CO}^{c} = S_{\rm CO}^{\rm min} + 5 \, \sigma(S_{\rm CO}) \, ,$$

where

$$\sigma(S_{\rm CO}) = \sigma \Delta V \sqrt{N_p N_c / 17.55}$$

and σ is the rms noise in the map, N_p is the minimum number of pixels required for a detection, and N_c is the minimum number of velocity channels required for a detection. For $\sigma = 0.055$ Jy beam^{-1}, $N_p = 4$, and $N_c = 1$, we get $\sigma(S_{\rm CO}) = 0.14$ Jy km s^{-1}, which gives a 5 σ completeness limit of 0.86 Jy km s^{-1}, or a mass limit of 5.0×10^6 $M_\odot$.

We made least-squares fits to the six mass functions, including $\sqrt{N}$ uncertainties and ignoring bins with $\log M \leq 6.7$. The slope and the uncertainty in the slope are included in Figure 3. The average slope across the three different identification runs is $\alpha = -1.4 \pm 0.1$. This slope refers to a mass range from 5×10^6 to $\sim 10^9$ $M_\odot$ and is significantly shallower than the canonical stellar initial mass function derived by Salpeter (1955; −2.35 on the same scale). However, this slope of −1.4 is very similar to the slope of −1.5 obtained for the mass function of giant molecular clouds in the Milky Way (Sanders et al. 1985; Solomon et al. 1987). It is somewhat shallower than the slope of −1.8 found over a mass range 1000 to 10^6 $M_\odot$ for molecular regions in the outer Galaxy (Heyer et al. 2001). However, Heyer et al. (2001) point out that many of the low-luminosity objects in their survey are not self-gravitating, in which case the mass function may be shallower than the luminosity function. In addition, the relatively poor spatial resolution of our Antennae data means that blending of individual clouds into a single feature could be an important effect, which would tend to make our observed mass function shallower than the true mass function. Kramer et al. (1998) also obtained similar slopes ranging from −1.6 to −1.8 from CO observations of clumps inside seven molecular clouds. The clump masses in their sample ranged from as low as 10^{-4} $M_\odot$ to as high as 10^4 $M_\odot$ and overlap at the high-mass end with the mass range covered by Heyer et al. (2001). (However, steeper clump mass functions, consistent with the

stellar initial mass function over a fairly narrow mass range from ~0.5 to ~10 $M_\odot$, have been derived recently for several nearby clouds by using submillimeter continuum data; Testi & Sargent 1998; Motte, André, & Neri 1998; Johnstone et al. 2000; Motte et al. 2001.) Thus, by combining our new study of the Antennae with previous work on the Milky Way, we see that the mass function of structures in the molecular interstellar medium in galaxies has a fairly constant slope of about -1.5 ± 0.2, which extends over at least 8–9 orders of magnitude in mass, from 1–10 up to 10^9 $M_\odot$. It is worth noting that these power-law mass spectra are consistent with a model in which clouds grow by agglomeration from smaller objects (Kwan 1979).

3.2. *Previous Observations of Molecular Complexes in Other Galaxies*

We have searched the literature for CO observations of galaxies with spatial resolution of better than 1 kpc to see what is known about massive molecular complexes in other galaxies (Table 1). Objects similar to the most massive complexes in the Antennae have been found in only three other galaxies: NGC 1068 (Planesas, Scoville, & Myers 1991), Arp 220 (Sakamoto 1996), and Arp 299 (Casoli et al. 1999). By adopting a distance of 14.4 Mpc for NGC 1068 (Tully & Fisher 1988), the most massive complex is 4.5×10^8 $M_\odot$ (Planesas et al. 1991), and the average molecular gas surface density in the inner arcminute is roughly 100 $M_\odot$ pc^{-2}, both comparable to what is seen in the Antennae. In Arp 220 and Arp 299, the massive gas concentrations are located in the galactic nuclei, which probably makes them more similar to the gas located in the nucleus of NGC 4038 than the molecular complexes in the disks and overlap region. In the remaining normal spiral galaxies for which high-resolution CO observations have been made, the most massive complex ranges from as small as 1.6×10^7 $M_\odot$ in M83 (Rand, Lord, & Higdon 1999) to as large as 1.3×10^8 $M_\odot$ in M100 (Rand 1995). For the five galaxies in Table 1 with distances between 9 and 19 Mpc, the angular resolution of the data sets varies by only a factor of 2, while the mass of the most massive complex varies by a factor of almost 20. This result suggests that the large complexes seen in the Antennae and in NGC 1068 are not the result of cloud blending due to the relatively large distances of these two galaxies.

In only two galaxies, M51 (Rand & Kulkarni 1990) and NGC 1068 (Planesas et al. 1991), are sufficiently large numbers of objects detected that it is possible to look at the mass function of the molecular complexes. However, the limited mass range of the molecular complexes in M51 [$(1–6) \times 10^7$ $M_\odot$] makes it impossible to determine the slope with any degree of accuracy. The 38 complexes detected in NGC 1068 range from 2×10^7 to 7×10^8 $M_\odot$. Fitting the entire mass range in the same manner as was done for the Antennae data gives a slope of -1.3 ± 0.2 for the differential mass function, which is quite similar to that obtained in the Antennae. From this comparison with previous studies of other galaxies, it is clear that the population of molecular complexes identified in the Antennae both is the largest sample and covers the largest dynamic range in mass. It would be interesting to carry out deeper observations of Arp 220 and Arp 299 to see whether the mass functions of the molecular complexes in these more advanced interacting systems are similar to those measured for the Antennae and NGC 1068.

3.3. *Spatial Relationship between Young Massive Star Clusters and Supergiant Molecular Complexes in the Antennae*

Whitmore et al. (1999) have published a large sample of young massive star clusters observed with the Wide Field Planetary Camera 2 (WFPC2) on the *Hubble Space Telescope*. They find that the overlap region contains primarily clusters with ages less than 5 Myr. This region contains roughly half the total amount of molecular gas detected in our map and has correspondingly very high extinctions, with an average A_V of 96 mag toward the three brightest CO peaks in this region. Thus, any clusters identified in this part of the overlap region must lie on the near side of the molecular complexes. The western loop of gas and young stars to the west of NGC 4038 contains clusters with ages primarily in the range 5–10 Myr. In this region, the CO emission occurs primarily between regions of many young clusters (Fig. 4), and the typical extinction toward a cloud in this region is $A_V \sim 13$. A very interesting region

TABLE 1
MASSIVE MOLECULAR COMPLEXES IN OTHER GALAXIES

Galaxy	Beam Size (pc)	Distance (Mpc)	Maximum Mass (10^8 $M_\odot$)	Notes	References
M83	110 × 55	3.3	0.1	10 complexes	1, 2
NGC 5055	220 × 170	7.2	0.5	17 complexes	3, 4
M51	370 × 290	8.6	0.5	26 complexes	5, 6
NGC 1068	210 × 210	14.4	4.5	38 complexes	7, 4
M100	360 × 280	16	1.2	7 complexes	8, 9
NGC 4414	480 × 480	19	0.4	8 complexes	10, 11
NGC 4038/4039	480 × 310	19	8.9	86 complexes	12, 13
Arp 299	750 × 510	42	40	Nucleus of IC 694	14, 13
Arp 220	210 × 190	77	10	Nucleus, X_{CO} uncertain	15, 13

NOTE.—Masses have been scaled to the same CO-to-H_2 conversion factor used in this paper, except for Arp 220, for which a value 2.5 times smaller was used.

REFERENCES.—(1) Rand, Lord, & Higdon 1999; (2) Distance to group member NGC 5253 from Gibson et al. 2000; (3) Thornley & Mundy 1997; (4) Tully & Fisher 1988; (5) Rand & Kulkarni 1990; (6) Feldmeier et al. 1997; (7) Planesas et al. 1991; (8) Rand 1995; (9) Ferrarese et al. 1996; (10) Sakamoto 1996; (11) Turner et al. 1998; (12) this paper; (13) $H_0 = 75$ km s^{-1} Mpc^{-1}; (14) Casoli et al. 1999; (15) Sakamoto et al. 1999.

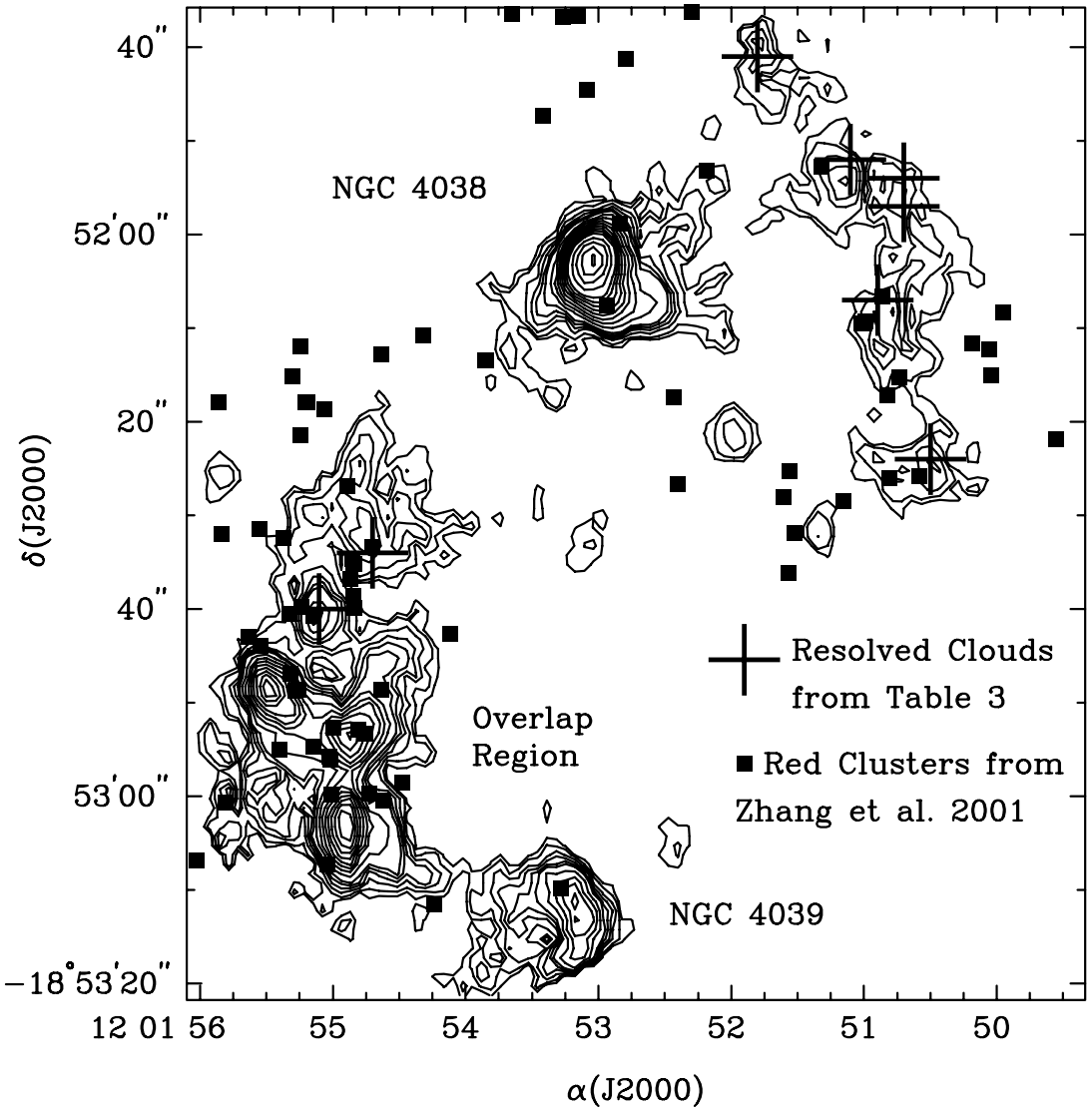

FIG. 4.—Locations of young red superstar clusters using the coordinates from Zhang, Fall, & Whitmore (2001), overlaid on the CO contours from Fig. 1*b*. Roughly 40% of these clusters are found in the overlap region, which covers only 10% of the area of the total CO map. However, some young clusters are found as far as 1–2 kpc from strong CO emission, which suggests that they either formed from a lower mass molecular complex or that they have already destroyed their parent cloud. The locations of the eight resolved clouds from Table 3 are also indicated.

from the point of view of cluster formation is the northeastern portion of NGC 4038. Whitmore et al. (1999) find that this region contains many young massive star clusters, with two-thirds of the clusters having ages less than 30 Myr and one-third having ages around 100 Myr. The presence of the younger star cluster population is interesting given the total lack of detected CO emission in this part of our map. Our 5 σ detection limit of $5 \times 10^6\ M_\odot$ (§ 3) means that only relatively normal giant molecular clouds can be present in this region of the galaxy.

Zhang, Fall, & Whitmore (2001) have compared the locations of three age groups of star clusters with data at a variety of other wavelengths. They find that clusters with ages less than 5 Myr (the reddest clusters) are more associated with wavelengths longer than mid-infrared, while clusters with ages greater than 10 Myr are more closely associated with far-ultraviolet and X-ray emission. The two-point correlation function for the red clusters is a power law up to a radius of 0.74 kpc. The maximum size of the power-law portion of the correlation function is very similar to the sizes of the supergiant molecular complexes, which suggests that an upper limit to the correlation function could correspond to a set of clusters formed inside a single such complex. Zhang et al. (2001) estimate a total star formation rate from Hα emission (corrected for 1.8 mag of extinction and assuming a Salpeter initial mass function from 0.1 to 100 $M_\odot$) of 20 $M_\odot\ \mathrm{yr}^{-1}$. This star formation rate is a factor of 2 larger than the star formation rate of 10 $M_\odot\ \mathrm{yr}^{-1}$, which can be derived from the far-infrared luminosity, following Kennicutt (1998).

We compare the locations of the young red star clusters discussed in Zhang et al. (2001) with the distribution of the molecular gas in Figure 4. Roughly 40% of these young obscured clusters lie within the region of strong CO emission in the overlap region, which occupies only 10% of the total area mapped in CO. Thus, we confirm the conclusions of Zhang et al. (2001) that the youngest clusters are significantly correlated with regions containing molecular gas.

However, some of these youngest star clusters lie a significant distance from strong CO emission, up to 1–2 kpc in regions to the north and east of the galaxies. This result is also true for the older B1 and B2 cluster groups (compare Fig. 4 with Fig. 2 of Zhang et al. 2001). Since our CO map does not contain all the CO flux of these galaxies, it is possible that significant molecular gas exists near these otherwise isolated young clusters. However, this molecular gas must be in rather lowmass clouds to have avoided detection in our map; in particular, any remaining clouds associated with these clusters are likely to have masses less than $5 \times 10^6\ M_\odot$, our 5 σ detection limit for clouds. Comparing the CO and cluster distributions thus suggests either that relatively lowmass molecular clouds can form the occasional massive star cluster, that massive star clusters can destroy their parent clouds on a rather rapid timescale, or both.

4. CASE STUDY COMPARISON WITH M51

To illustrate better the unusual aspects of the molecular interstellar medium in the Antennae, we compare the total gas mass and the properties of the molecular complexes and young massive clusters with the grand-design spiral galaxy M51. (Unfortunately there seem to be no surveys for young massive star clusters in NGC 1068, which would otherwise be another interesting galaxy to compare with the Antennae.) Rand & Kulkarni (1990) mapped a $4' \times 5'$ region of the inner disk of M51 with the three-element Caltech Millimeter Array and detected 26 giant molecular associations with masses ranging from 1×10^7 to 5×10^7 $M_\odot$. The beam size ($9'' \times 7''$, or 370×290 pc at a distance of 8.6 Mpc; Feldmeier, Ciardullo, & Jacoby 1997; Ferrarese et al. 2000) is a very good match to our study of the Antennae. To match the total area surveyed as well, we restrict our analysis to clouds within a 5 kpc radius of the nucleus of M51. Correcting for the larger distance to the Antennae, our study is 1–2 times more sensitive to a complex of a given mass than is the M51 study of Rand & Kulkarni (1990). To correct for this difference in mass sensitivity, we further restrict our comparison to complexes that have masses larger than $2 \times 10^7\ M_\odot$. More recent work by Aalto et al. (1999) provides better resolution and sensitivity for M51, but we prefer to use the older study of Rand & Kulkarni (1990) because it provides a better match in spatial resolution and mass sensitivity to our Antennae data.

M51 contains 13 molecular complexes with masses greater than $2 \times 10^7\ M_\odot$ inside an area of 79 kpc^2. In contrast, the Antennae contain 43 complexes with masses greater than $2 \times 10^7\ M_\odot$ inside the same area. Thus, the Antennae have a 3 times higher surface density of massive molecular complexes than does M51. (However, correction for the poorly known inclination of the disks of NGC 4038 and NGC 4039 might reduce this ratio by up to a factor of 2.) In addition, the most massive complex seen in M51 has a mass of $5 \times 10^7\ M_\odot$, while the most massive complex in the Antennae (ignoring the gas in the nucleus of NGC 4038) has a mass of $6 \times 10^8\ M_\odot$, 12 times more massive than that seen in M51. Thus, while the Antennae have a somewhat higher surface density of massive molecular complexes than does M51, the most striking aspect of the molecular complexes in the Antennae is that their mass function extends to much larger masses than are seen in M51. If the molecular complexes in both galaxies follow a similar power-law mass function, then fitting the data with truncated power laws following the prescription of Scoville et al. (2001) shows that the M51 mass function is significantly truncated. In particular, given that 13 complexes are observed with masses greater than $2 \times 10^7\ M_\odot$, we would expect to see four complexes with masses greater than $6 \times 10^7\ M_\odot$. Thus, it is probably not small number statistics that is imposing the upper mass limit in M51.

It is important to compare the total amount of molecular gas in the Antennae and M51 to see whether the presence of very massive complexes can be attributed to a larger total reservoir of molecular gas to form them. Within the region of our study, Gao et al. (2001) measure a total mass of $9.6 \times 10^9\ M_\odot$ (§ 2). This mass corresponds to a surface density of 120 $M_\odot$ pc^{-2} (again with no correction for inclination, which could reduce this value by as much as a factor of 2). Garcia-Burillo, Guélin, & Cernicharo (1993) made a large map of M51 by using the IRAM 30 m telescope; within the central 79 kpc^2 and using a conversion factor that is 3 times smaller than the value adopted here for the Antennae, their measurements correspond to a total mass of molecular gas of $6 \times 10^9\ M_\odot$, or a surface density of 90 $M_\odot$ pc^{-2}. Thus, within uncertainties due to inclination in the Antennae and the CO-to-H_2 conversion in M51, the total molecular gas surface density appears comparable in the two galaxies and certainly not different enough to account for the formation of extremely massive molecular complexes in the Antennae.

One important difference between the two galaxies is their velocity fields. Figure 2 shows that the Antennae have a reasonably regular velocity field in the northwestern arc, which may represent a fairly unperturbed piece of the disk of NGC 4038. However, the velocity field in the overlap region appears extremely disturbed; instead of a smooth progression in velocity, there are two large regions with fairly constant velocities separated by a boundary with a steep velocity gradient. In contrast to the disturbed velocity field of the Antennae system, the velocity field in M51 shows evidence of streaming motions due to the presence of spiral density waves superposed on a very regular rotation pattern (Aalto et al. 1999). This marked difference in the velocity fields in M51 and the Antennae (which is not unexpected given the strong interaction in the Antennae) suggests a possible explanation for the presence of very massive molecular complexes in the Antennae. In a regularly rotating disk, molecular clouds that contain enough mass to be gravitationally bound may be subject to disruption by the effects of tides and shear (Rand 1993). Thus, it is possible that the formation of very massive gas clouds is suppressed in M51 because of high shear in its differentially rotating disk. The effect of galaxy mergers such as the Antennae on the shear in the galactic disks is not well understood, although it seems possible that some regions undergo increased shear, while other regions may experience reduced shear. It is interesting that for NGC 1068 (the other nearby spiral galaxy with massive gas clouds), Schinnerer et al. (2000) have suggested that the gaseous spiral arms may lie at the inner Lindblad resonance of a much larger (17 kpc) bar. Thus, the massive gas clouds in NGC 1068 may also have formed in a region of reduced shear.

Surveys for young massive star clusters in M51 have been carried out recently by Larsen (2000) and Lamers et al. (2002). Using ground-based imaging, with *Hubble Space Telescope* (*HST*) archival confirmation of 10 clusters,

Larsen (2000) identified a population of 69 candidate young clusters with ages less than 500 Myr. This sample contains 40 clusters with $M_V < -10$ mag and four clusters with $M_V < -12$ mag. Lamers et al. (2002) used *HST* WFPC2 imaging of the nuclear region of M51 to identify a sample of 30 pointlike sources. However, they concluded that these sources were most likely to be single stars or very small ($M <$ a few 100 $M_\odot$) star clusters rather than massive star clusters. At the extremely young end of the scale, Scoville et al. (2001) concluded from their Paα and Hα surveys that the most massive star cluster in M51 that is ionizing an H II region has a mass less than 5000 $M_\odot$. Larsen (2000) notes that M51 is rich in young massive star clusters compared with an average spiral galaxy, but that it is not *unique* in its rich star cluster population.

In comparison, in just a single 10 kpc^2 region of the Antennae Whitmore et al. (1999) find a total of seven clusters with $M_V < -12$ mag. Although this region of the Antennae is particularly rich in clusters, it seems likely that the Antennae as a whole contain an order of magnitude more of the most luminous clusters than does M51. A total of 14,000 point sources have been identified in the Antennae (Whitmore et al. 1999), of which at least 40% are contaminating stars and at least 800 are definitely star clusters. Zhang & Fall (1999) identify 2000 star cluster candidates from this sample that lie within 0.3 mag of cluster evolutionary tracks and have $M_{V,0} < -9$ mag. Compared with the $\sim$70 star clusters identified in M51 by Larsen (2000), these observations suggest that the Antennae contain at least 30 times as many star clusters as M51. This difference is even more striking when we consider the average star formation rates in the two galaxies. The star formation rate is roughly proportional to the far-infrared luminosity (i.e., Kennicutt 1998); M51 has a far-infrared luminosity of 1.8×10^{10} $L_\odot$ (Rice et al. 1988), while the far-infrared luminosity in the Antennae is 5.6×10^{10} $L_\odot$ (Gao et al. 2001), roughly 3 times larger than in M51. Thus, in comparison with their star formation rates, the Antennae contain an order of magnitude more young massive star clusters than does M51. We suggest in § 6 that the formation of young massive clusters in the Antennae is enhanced by its ability to form very massive gas clouds.

5. ARE THE ANTENNAE UNDERGOING A SHORT-LIVED STARBURST?

5.1. *Recent Star Cluster Formation Rates from Optical and Radio Data*

We can derive clues to the recent star cluster formation rate in the Antennae by examining the number of massive star clusters as a function of age. We can also use radio continuum observations to estimate the number of very young embedded star clusters and older supernova remnants (Neff & Ulvestad 2000). The mass function analysis of Zhang & Fall (1999) shows that there are roughly 300 young star clusters more massive than 10^5 $M_\odot$ in the Antennae. Of these clusters, roughly 100 fall in the young age range 2.5–6.3 Myr, and a similar number fall in the age range 25–160 Myr. There are two simple explanations for the similar number of star clusters observed in these very different size age bins. If the observed number of star clusters reflects the average cluster formation rate over each time period, then the cluster formation rate in the last 6 Myr must have been 20 times higher than the cluster formation rate over the previous 150 Myr. However, this picture implies a very rapid change in the cluster formation rate compared with the current crossing time of the system ($\sim$100 Myr; Mihos, Bothun, & Richstone 1993). Alternatively, if the cluster formation rate has been constant over the last 150 Myr, then roughly only one out of 20 of the younger clusters can survive in the long term (Zhang & Fall 1999; Whitmore 2002). Mengel et al. (2002) have measured dynamical masses for five bright clusters in the Antennae, which suggests that these clusters are gravitationally bound and hence likely to survive. However, we have no information about the likelihood of survival for the vast majority of the star clusters in the Antennae. A counterexample of a luminous star cluster that seems to have insufficient low-mass stars to survive can be found in M82 (Smith & Gallagher 2001).

A recent high-resolution radio survey shows that the Antennae contain 13 sources with obviously thermal spectral energy distributions that likely have ages in the range 1–3 Myr (Neff & Ulvestad 2000). These sources contain an equivalent mass in stars between 0.1 and 60 $M_\odot$ (assuming a Salpeter initial mass function) of 2×10^5 to 1×10^7 $M_\odot$.[6] Roughly accounting for sources that have been missed because of large uncertainties on their spectral index, as well as slightly less massive sources, we estimate that the number of optically thin thermal sources with masses greater than 10^5 $M_\odot$ is perhaps 30. In comparison, there are roughly 100 star clusters more massive than 10^5 $M_\odot$ with ages $\leq$6 Myr (Zhang & Fall 1999). Thus, the number of optically visible star clusters and the number of optically thin thermal sources appear to be consistent with a constant star cluster formation rate in the Antennae over the last 6 Myr.

These numbers are also consistent with the result from Whitmore & Zhang (2002), who find that essentially all the bright thermal radio sources can be identified with optically visible star clusters. This good match between the radio and optical sources is rather puzzling in the overlap region, where the visual extinction can reach as high as 100 mag (§ 3.3). However, a closer examination of the sources in the overlap region reveals that all sources except WS 80 lie well away from the brightest CO peaks. WS 80 itself is coincident with SGMC 7, which has an average visual extinction of 25 mag. Whitmore & Zhang (2002) estimate a visual extinction for WS 80 of 7.6 mag, which is consistent with it lying fairly close to the center of this somewhat lower mass molecular cloud.

Turning now to the supernova rate, which traces star formation over slightly longer time periods, Neff & Ulvestad (2000) used the observed flux in nonthermal radio sources to estimate a current supernova rate of 0.1–0.2 yr^{-1}. This rate is a factor of 10–20 larger than the 0.01 yr^{-1} that they estimate from the number of O5 stars and the lifetime of these stars. This result led them to postulate that the Antennae suffered a very sharp burst of star formation 3–4 Myr ago that lasted only a few hundred thousand years. However, the 60 $M_\odot$ O5 stars are not the only stars that produce supernovae; conservatively, all stars with masses

[6] These masses can be obtained by scaling the mass in O5 stars by a factor of 45, assuming ionizing luminosity $L_i \propto m^{3.5}$, $L_i(\mathrm{O5}) = 4.7 \times 10^{49}$ ergs s^{-1}, and $M(\mathrm{O5}) = 60$ $M_\odot$ (J. S. Ulvestad 2002, private communication).

greater than 20 $M_\odot$ can produce a supernova. There are many more of these lower mass O stars, but they have significantly longer main-sequence lifetimes. However, if the star formation rate has been constant over the longer lifetimes of these stars, then the numbers of O stars will approach a steady state, with the number of stars at any mass proportional to the product of the initial mass function and the lifetime of the stars. This effect will increase the supernova rate over that calculated by Neff & Ulvestad (2000). For example, if the stellar lifetime were to vary as $t \sim m^{-1.65}$, then the number of supernovae produced by 20–50 $M_\odot$ stars would be 35 times the number produced by 50–60 $M_\odot$ stars. Thus, depending on the exact relationship between mass and lifetime and the lower mass limit for producing a supernovae, it appears that the observed supernova rate in the Antennae is roughly consistent with a constant star formation rate over the last 10–20 Myr.

Given the results from the comparison with the radio data, it seems reasonable to assume that the star cluster formation rate over the last 160 Myr was roughly constant but that only a small fraction of the clusters formed 160 Myr ago survive to the present time (Fall & Zhang 2001). This scenario would involve forming $\sim$2000 clusters over the last 160 Myr with a total initial mass in the clusters of $\sim 10^9\ M_\odot$. This large mass is still only a small fraction of both the total mass of molecular gas (Gao et al. 2001) and the total luminous mass in the Antennae. Thus, the amount of gas available to fuel star formation in the Antennae does not require that the current epoch of intense star cluster formation be confined to a very short period of time. A model with a roughly constant cluster formation rate is consistent with a picture in which the starburst activity in the Antennae is dynamically triggered, in which case we would not expect the star formation rate and star cluster formation rate to change on a much shorter timescale than the dynamical time, or on the order of 100 Myr (Mihos et al. 1993).

5.2. *Future Rate of Cluster Formation in the Antennae*

We estimate the *future* rate of star cluster formation in the Antennae by using a model based on our knowledge of current star formation in the Milky Way. If supergiant molecular complexes are similar in their star formation properties to giant molecular clouds in the Milky Way, then we might assume that they form at most 5% of their mass into stars. By analogy with what is seen in the Orion molecular cloud (Lada et al. 1991b), we would expect these stars to form predominantly in star clusters. Given that the total mass in supergiant molecular complexes is $6 \times 10^9\ M_\odot$, we might expect them to form a total mass of star clusters of up to $3 \times 10^8\ M_\odot$. Zhang & Fall (1999) find that the mass function of the young massive clusters in the Antennae follows a power law with a slope of -2. This mass function implies that there is an equal amount of mass in equal logarithmic mass bins, and thus the number of clusters more massive than $10^5\ M_\odot$ depends on the lower mass cutoff to the mass function. For example, if star clusters form over a mass range from 10^4 to $10^6\ M_\odot$, then the mass function will contain 600 clusters more massive than $10^5\ M_\odot$, whereas if star clusters form over a mass range from 100 to $10^6\ M_\odot$, the number of massive clusters would be only half as large. These rough estimates suggest that we might expect the existing supergiant molecular complexes in the Antennae to form between 300 and 600 star clusters more massive than $10^5\ M_\odot$. These clusters likely form over at least a crossing time, which for the largest complex is 30 Myr. This implies a massive star cluster formation rate of 10–20 Myr^{-1}, which is approximately the same rate as is seen in the youngest star cluster sample of Zhang & Fall (1999).

If clusters older than 30 Myr have been subject to destruction, it is possible that the Antennae have been experiencing a high and uniform rate of star cluster formation over the last 100–200 Myr and could possibly sustain this formation rate for at least another 30 Myr. What might happen after that? If the molecular gas can re-form itself into supergiant molecular complexes (or other structures) capable of forming massive star clusters over that same timescale, then massive star cluster formation could continue at the same rate until all the gas is exhausted. However, the northeast region of NGC 4038 suggests that, once a region has formed many young massive star clusters, it is unlikely to be ready to form them again just 30 Myr later. On the other hand, the fact that we see star clusters forming now in the overlap region suggests a mode of star formation in which a portion of the galaxy lights up in young clusters formed 30 Myr ago, while another portion of the galaxy is forming the next generation of clusters. Perhaps the western arc represents an intermediate-age region where we still see gas and star clusters intermingled. In this picture, a continuous period of star cluster formation extending well in excess of 30 Myr but isolated to only a portion of the galaxy at a time could perhaps be sustained. If this mode of cluster formation continued for as long as 600 Myr, the Antennae would form 6000–12,000 clusters, of which as few as 300–600 might survive in the long term. Slow infall of atomic material from the tidal tails (Hibbard et al. 2001; Hibbard & Mihos 1995) could help prolong the period of active star cluster formation.

We need to consider whether the expected total star cluster formation rate in this simple model would cause the Antennae to exceed the typical specific frequency for globular (and other) clusters in an elliptical galaxy. The current V-band absolute magnitude of the Antennae system is about -22 (from data in LEDA). The "normal" value for the specific frequency is about 3.5 (Harris 2001), which means we would expect to find a total of about 2200 clusters more massive than $10^5\ M_\odot$ in an elliptical galaxy with $M_V = -22$ mag. If the Antennae were to fade by 1.5 mag in the process of forming an elliptical galaxy (Whitmore & Schweizer 1995), then the expected number of clusters would be 600. Whether these numbers agree in detail with the model discussed above depends on both the duration of cluster formation and how many of the young massive star clusters survive over the long term. There is no difficulty if only 5%–10% of the young massive star clusters that could be formed in future from the molecular gas reservoir survive as clusters after 1 Gyr. However, if all the young (2–6 Myr) massive star clusters that we see now survive to old age, we would have to be witnessing an extremely short-duration starburst for the final specific frequency of the Antennae not to exceed (by a wide margin!) the typical specific frequency seen in elliptical galaxies. In this context, it is relevant that somewhat older ($\sim$1 Gyr) mergers such as NGC 3921 (Schweizer et al. 1996) and NGC 7252 (Milleret al. 1997) are likely to end up with specific frequencies that fall in the normal range of field elliptical galaxies.

6. FORMING MASSIVE STAR CLUSTERS: CONSTRAINTS FROM THE GAS PROPERTIES

6.1. *Two Contrasting Models for Massive Star Cluster Formation*

Larsen & Richtler (2000) show that the fraction of the *U*-band luminosity that originates in young star clusters is proportional to the star formation rate per unit area in a galaxy. Roughly speaking, their result suggests that if you double the surface density of star formation, you double the fraction of the galaxy luminosity that occurs in star clusters. The luminosity in star clusters depends in a complicated way on the star formation history of a galaxy, as well as on the survival rate of the star clusters. However, using the *U*-band luminosity function preferentially selects clusters that are typically less than 30 Myr old, which is comparable to the timescale over which the star formation rate is traced via Hα imaging. Larsen (2000) concludes that galaxies form young massive star clusters wherever the star formation rate is high enough. He suggests that this could be linked to the formation of giant molecular associations, which may assemble more easily in galaxies with a higher gas surface density. However, our comparison of M51 and the Antennae in § 4 shows that they have similar gas surface densities and yet have very different star cluster populations, so gas surface density cannot be the only important parameter in the formation of young massive star clusters.

Various models have been proposed to explain the formation of young massive star clusters. Schweizer et al. (1996) have noted the similarity between the masses of the young star clusters and the masses of giant molecular clouds in the Milky Way (10^4–10^6 $M_\odot$). However, the radii of the two objects are quite different, with the young massive star clusters having effective radii of 4 pc (Whitmore et al. 1999) and giant molecular clouds having radii in the range 5–50 pc, depending on their mass. Schweizer et al. (1996) have suggested that a young massive star cluster could be formed through shock compression of a giant molecular cloud to force the cloud to form stars with an efficiency of $\sim$50%, much higher than the star formation efficiencies of a few percent that are typically seen (Evans & Lada 1991). They suggest that one means by which giant molecular clouds could possibly be compressed is through the formation of a hot high-pressure interstellar medium during galaxy collisions (Jog & Solomon 1992). This model was originally developed to explain the formation of a starburst during galaxy interactions. In the model, the outer layers of a giant molecular cloud are compressed by contact with hot shocked H I clouds and form stars with a high efficiency. However, the amount of the cloud mass that is subject to this high efficiency is estimated to be 10% and would be distributed in a shell-like structure rather than a compact spherical structure. In addition, to match the observed parameters of starburst galaxies, in particular their high infrared luminosity, Jog & Solomon (1992) assume that only stars more massive than 1 $M_\odot$ are formed in this process. Thus, this model does not seem to be directly applicable to the formation of compact massive star clusters.

An alternative model that has been proposed to explain the formation of globular clusters (Harris & Pudritz 1994; McLaughlin & Pudritz 1996) may be applicable to the formation of young massive star clusters in galaxy mergers. This model supposes that globular clusters formed by the same type of process that we see forming star clusters today. However, the large masses of globular clusters compared with star clusters in clouds such as Orion require that the globular clusters form within molecular clouds that are substantially larger than the molecular clouds in the Milky Way. For example, the Orion B molecular cloud has a total mass of 8×10^4 $M_\odot$ and contains five molecular cores with masses ranging from 100 to 450 $M_\odot$ (Lada, Bally, & Stark 1991a). Four of these cores are forming infrared star clusters with a star formation efficiency of 50% (Lada et al. 1991b), and most of the star formation is occurring in these cores. If a globular cluster (or a young massive star cluster) formed inside a larger molecular core with a star formation efficiency of 50%, this would require cores with masses from 2×10^5 to 2×10^6 $M_\odot$. If these large cores were contained within a larger cloud with a core-to-cloud mass ratio similar to Orion B, the cloud mass required to contain these cores would be 4×10^7 to 4×10^8 $M_\odot$. These cloud masses are very similar to those of the supergiant molecular complexes we have identified in the Antennae. Note that in this model we would expect each supergiant molecular complex to contain several massive cores and hence to form several massive star clusters over its lifetime.

6.2. *Role of Pressure in the Two Models*

One possible way to distinguish between these two models may be via the environment in which the clouds live, particularly the pressure. We can estimate the pressure in a few regions in the Antennae from the recent work by Fabbiano et al. (2003). They have made *Chandra* observations that are sufficiently sensitive to be able to fit the physical conditions in the hot interstellar medium in the two nuclei and also in a region in the western star-forming arc. Assuming a scale height of 200 pc for the high-temperature component, the pressure in each of these regions is in the range $(4\text{–}8) \times 10^5$ K cm^{-3}, with an average over the three regions of 6×10^5 K cm^{-3}. This pressure is significantly larger than the typical interstellar medium pressure in the Milky Way of 10^4 K cm^{-3} (Elmegreen 1989). If the pressure in these three regions is typical of the Antennae disk as a whole, then the supergiant molecular complexes in the Antennae are embedded in a higher pressure environment than are molecular clouds in the Milky Way.

How does this observed pressure compare with the models of star cluster formation discussed previously? Harris & Pudritz (1994) adopt a surface pressure for molecular clouds that is 10 times larger than the typical interstellar medium pressure to account for the effect of embedding H I envelopes. Using the formula in Elmegreen (1989) and H I data from Hibbard et al. (2001), the pressure due to the average atomic gas column density in the Antennae is only $\sim 10^4$ K cm^{-3}, closer to the Milky Way pressure than any other component of the interstellar medium in the Antennae. Thus, the surface pressure felt by the supergiant molecular complexes in the Antennae is likely to be in the range 6×10^5 to 6×10^6 K cm^{-3}, depending on whether they are surrounded by massive H I envelopes with pressures significantly above the average pressure in the atomic gas. Since the radius of a cloud varies as $P^{-1/4}$, a cloud of 3×10^8 $M_\odot$ should have a radius between 300 and 600 pc. This size is a reasonable match to those of the molecular complexes in the Antennae. The model of Jog & Solomon (1992) predicts a pressure of 10^8 K cm^{-3} in the hot shocked H I clouds. Although this pressure is substantially higher

than that estimated from the X-ray data, the expected filling factor of this hot gas is less than 1%. With this low filling factor, the average pressure predicted in the model is 6×10^5 K cm^{-3}, which is quite similar to the X-ray data. Thus, it seems that the pressure of the interstellar medium in the Antennae cannot help us to distinguish between the two models.

Even the high pressures inferred from the X-ray data for the Antennae are still substantially smaller than the typical pressure inside a single self-gravitating molecular complex. The average pressure in SGMC 3 is 2×10^6 K cm^{-3}, while the central pressure is in the range 10^6–10^7 K cm^{-3}, depending on the exact geometry. Indeed, the pressure inside the ρ Oph core, a relatively small star-forming cloud in the Milky Way, is 10^7–10^8 K cm^{-3} (Johnstone et al. 2000). Elmegreen & Efremov (1997) estimate the pressure required to form a typical globular cluster to be in the range 10^6–10^8 K cm^{-3}.

6.3. *Applying the Models to the Nonmerger Environment*

It is important to see whether we can understand the formation of young massive star clusters in noninteracting galaxies in the context of these two models. A particularly useful case study is the R136 star cluster in the LMC. The total mass of stars in R136 is estimated to be 6×10^4 $M_\odot$ (Hunter et al. 1995), and the age of the star cluster is at most 1–2 Myr (Massey & Hunter 1998). There appears to be no molecular gas in the immediate environment of R136 (Johansson et al. 1998); however, there is a very extended region of CO emission to the south of R136 (Cohen et al. 1988). If we consider this entire region as a single large structure, it has a size of 400×1200 pc and a total mass of about 9×10^6 $M_\odot$ (adopting the appropriate CO-to-H_2 conversion factor from Wilson 1995). Adopting the velocity width of 10.5 km s^{-1} measured by Kutner et al. (1997), the virial mass of this region is 1.5×10^7 $M_\odot$, or within a factor of 2 of the flux-based mass. Thus, this large CO complex may be gravitationally bound. If R136 formed in a core of 1×10^5 $M_\odot$, we would expect this core to have lived inside a larger cloud of mass 2×10^7 $M_\odot$, which is similar to the mass of the large CO complex. Thus, it seems reasonable to suggest that R136 might have formed from the most massive core of that molecular complex. R136 and 30 Dor are rather isolated at present from the main part of this molecular complex. However, the intervening region contains a number of H II regions and supernova remnants (Cohen et al. 1988), which could have acted along with R136 and 30 Dor to destroy much of the molecular gas over this larger region. Thus, the environment of the R136 cluster appears roughly consistent with the cluster formation picture put forward by Harris & Pudritz (1994), while the overpressure model advanced by Schweizer et al. (1996) seems less applicable here.

Returning now to M51, the CO data show that it currently contains 13 molecular complexes with masses in the range $(2–5) \times 10^7$ $M_\odot$ (Rand & Kulkarni 1990). Scaling again from Orion, we would expect the most massive core in each complex to be in the range $(1–3) \times 10^5$ $M_\odot$ and hence to be able to form a young star cluster with a mass up to $(1–2) \times 10^5$ $M_\odot$. The 69 star clusters identified by Larsen (2000) have ages less than 500 Myr. Depending on the masses of these star clusters (which have not been estimated) it seems quite possible for this relatively small population of clusters to have been formed from objects such as the lower mass molecular complexes seen in M51.

Young massive star clusters have been found even in relatively low luminosity dwarf irregular galaxies (Gelatt, Hunter, & Gallagher 2001; Hunter et al. 2000; Billett, Hunter, & Elmegreen 2002). Billett et al. (2002) note that, although it is rare for a dwarf galaxy to form luminous star clusters, when they do, they tend to form several clusters with similar ages. This result suggests that star cluster formation is concentrated to a localized region. Billett et al. (2002) emphasize that a lack of shear is probably the most important difference between dwarf irregular and spiral galaxies and suggest that triggered large-scale flows, possibly by an interaction, or ambient instabilities in a shear-free environment can make the clouds that form young massive star clusters in dwarf galaxies. Given the radically disturbed velocity fields seen in the Antennae, reduced shear might also be a factor in cloud formation in this system. An important difference between the Antennae and dwarf galaxies is the sheer size of the gas reservoir (Gao et al. 2001); perhaps combining a large gas reservoir with localized regions of reduced shear is the key to explaining the explosion of star cluster formation within the Antennae.

7. CONCLUSIONS

We have used sensitive CO $J = 1$–0 observations of the Antennae to study the detailed properties of the molecular clouds with the goal of understanding the prodigious formation of young massive star clusters in this nearby merger system. We have identified a total of $\sim$100 clouds in the data cube with masses ranging from 2×10^6 to 9×10^8 $M_\odot$. This sample of extragalactic molecular clouds is unique in the total number of clouds identified and in the mass range probed by the observations.

Above our 5 σ completeness limit of 5×10^6 $M_\odot$, the cloud mass function has a slope of -1.4 ± 0.1. This mass function slope is very similar to that seen in molecular clouds and molecular cloud cores in the Galaxy and is somewhat steeper than the mass function slope of -2 estimated for the luminous young star clusters in the Antennae by Zhang & Fall (1999). Our data suggest that the molecular interstellar medium in galaxies is governed by the same mass function slope over 8–9 orders of magnitude in mass, from 1–10 up to 10^9 $M_\odot$.

We have compared the Antennae with the nearby spiral galaxy M51, for which similar sensitivity and spatial resolution CO observations exist. Although the two galaxies have similar gas surface densities and total gas masses, the molecular clouds in M51 are an order of magnitude less massive than those in the Antennae. In addition, M51 has a much smaller population of young massive star clusters, perhaps 50 times smaller than that of the Antennae. One significant difference between the gas in the two galaxies is that M51 exhibits a smooth velocity field, while the velocity field in the Antennae is highly disordered. One possibility is that young massive star cluster formation in M51 is suppressed by its inability to form very massive gas clouds because of high shear in its differentially rotating disk.

Comparing the CO data with the locations of the youngest clusters shows that many of these clusters lie in the CO-rich overlap region. The extremely high extinction ($A_V \sim 100$ mag) toward the CO peaks means that the star clusters must lie in front of most of the molecular gas in this region. Interestingly, some of these youngest clusters are found as much as 2 kpc from regions with detectable

molecular gas. This result implies either that some young massive star clusters can form from clouds less massive than $5 \times 10^6\ M_\odot$, these clusters have already destroyed their parent molecular clouds, or both.

We have combined our CO data with published radio and optical data to sketch out the recent star formation history of the Antennae and to speculate on how star formation may proceed in the future. The relative numbers of very young massive star clusters and thermal and nonthermal radio continuum sources are consistent with a constant star formation rate over the last 10–20 Myr. If the star formation rate has been constant over the last 100 Myr, then the large number of star clusters with ages less than 10 Myr compared with those with ages of 20–100 Myr imply that a very large fraction of the star clusters formed must evaporate or be destroyed (Zhang & Fall 1999). On the other hand, if most star clusters survive for long periods, we would have to be witnessing an extremely short duration starburst for the final specific frequency of the Antennae not to exceed by a wide margin the typical specific frequency seen in elliptical galaxies.

The abundant supply of molecular gas seen in the extremely massive molecular clouds suggests that star cluster formation could easily proceed for at least a crossing time of one of these large clouds, or about 30 Myr. Indeed, the large reservoir of molecular gas measured by Gao et al. (2001) suggests that star cluster formation could continue for quite some time. The current distribution of gas and stars in the Antennae suggests a mode of star cluster formation in which portions of the galactic disks are lit up with recently formed clusters (for example, regions such as the northwestern arc), while other regions are forming the next generation of star clusters (currently in the overlap region).

We have compared our observations with two different models to explain the formation of young massive star clusters. The identification of extremely massive gas clouds in the Antennae means that the model of Harris & Pudritz (1994), which envisions globular cluster or super-star cluster formation as a scaled up version of Galactic star cluster formation, is a potentially viable model. The model advanced by Schweizer et al. (1996), which requires a source of high pressure to collapse preexisting giant molecular clouds to form stars with a much higher efficiency, may also be viable given recent constraints on the pressure in the Antennae from X-ray observations (Fabbiano et al. 2003). In addition, higher pressures can also be a feature of the Harris & Pudritz (1994) model, so that pressure alone cannot distinguish between the models. Understanding the formation of superstar clusters in dwarf galaxies, where there may not be a global source of enhanced pressure, may provide additional interesting constraints on this question. Ultimately, observations with new telescopes such as the Atacama Large Millimeter Array, which will have sufficient resolution and sensitivity to probe the small physical scales on which young massive star clusters form, will probably be required to fully understand this intriguing mode of star formation.

We thank the referee for useful comments, which improved the discussion, particularly in §§ 5 and 6. The research of C. D. W. is supported through grants from the Natural Sciences and Engineering Research Council of Canada. V. C. would like to acknowledge the support of JPL contract 960803. The Owens Valley Millimeter Array is operated by the California Institute of Technology and is supported by NSF grant AST 96-13717. C. D. W. acknowledges the hospitality of the Aspen Center for Physics and useful conversations with Susan Neff and Jim Ulvestad.

APPENDIX A

PROPERTIES OF INDIVIDUAL SUPERGIANT MOLECULAR COMPLEXES IN THE ANTENNAE

The properties of the individual supergiant molecular complexes (such as position, flux, and velocity) are given in Table 2. The clouds were identified using the program CLFIND with a contour level of 0.11 Jy beam^{-1} (2 σ), and their properties were measured using the program CLSTATS (Williams et al. 1994). The 5 σ mass sensitivity limit of the data set is $5 \times 10^6\ M_\odot$.

TABLE 2
GIANT MOLECULAR COMPLEXES IN THE ANTENNAE

ID[a]	α (J2000.0)	δ (J2000.0)	S_{CO} (Jy km s^{-1})	T_B[b] (K)	V_{lsr} (km s^{-1})	ΔV_{FWHM} (km s^{-1})	M_{mol} ($10^7\ M_\odot$)
20	12 01 53.1	−18 53 15	16.2	3.1	1683	21	9.4
86	12 01 53.1	−18 53 15	1.8	2.6	1755	6	1.0
22[c]	12 01 53.1	−18 53 14	23.2	4.0	1703	37	13.5
58[c]	12 01 53.2	−18 53 13	47.4	2.8	1610	56	27.5
72	12 01 55.1	−18 53 10	0.4	2.1	1641	5	0.2
32	12 01 54.2	−18 53 08	2.9	1.9	1464	16	1.7
79	12 01 53.7	−18 53 08	5.5	2.0	1683	27	3.2
65	12 01 53.7	−18 53 07	0.6	1.6	1620	9	0.3
7[c]	12 01 54.9	−18 53 06	11.2	3.5	1501	11	6.5
80	12 01 53.4	−18 53 05	0.9	1.9	1693	9	0.5
44	12 01 52.4	−18 53 04	1.4	2.5	1558	7	0.8
69	12 01 55.9	−18 53 04	1.3	2.8	1631	6	0.7
13	12 01 54.9	−18 53 03	2.1	2.3	1480	5	1.2

TABLE 2—*Continued*

ID[a]	α (J2000.0)	δ (J2000.0)	S_{CO} (Jy km s^{-1})	T_B[b] (K)	V_{lsr} (km s^{-1})	ΔV_{FWHM} (km s^{-1})	M_{mol} ($10^7\ M_\odot$)
12	12 01 54.6	−18 53 02	40.6	2.8	1485	53	23.6
8[c]	12 01 55.0	−18 53 01	42.6	3.8	1532	31	24.8
15[c]	12 01 54.9	−18 53 01	22.7	2.6	1568	49	13.2
9[c]	12 01 54.9	−18 53 01	11.3	3.7	1553	12	6.6
66	12 01 54.8	−18 52 59	4.7	1.8	1620	22	2.7
34	12 01 55.4	−18 52 58	5.4	2.2	1537	15	3.1
38	12 01 55.8	−18 52 58	0.4	2.3	1542	6	0.2
77	12 01 54.7	−18 52 56	2.5	1.5	1667	12	1.5
54	12 01 54.9	−18 52 55	1.4	2.0	1584	7	0.8
63	12 01 54.9	−18 52 55	0.4	1.5	1605	7	0.2
73	12 01 54.7	−18 52 55	1.8	1.5	1641	18	1.0
14	12 01 54.8	−18 52 54	4.3	2.1	1521	55	2.5
40	12 01 55.1	−18 52 54	0.3	1.6	1547	5	0.2
33	12 01 55.4	−18 52 54	1.6	1.9	1475	5	0.9
59	12 01 54.8	−18 52 53	2.4	2.0	1594	17	1.4
70	12 01 54.7	−18 52 53	0.4	1.4	1631	6	0.2
4[c]	12 01 54.8	−18 52 52	23.8	2.8	1449	23	13.8
5[c]	12 01 54.9	−18 52 52	44.0	3.4	1480	33	25.6
47	12 01 54.7	−18 52 52	2.3	1.4	1563	13	1.3
37	12 01 54.7	−18 52 52	0.9	1.5	1537	10	0.5
11	12 01 54.7	−18 52 50	8.6	2.2	1417	23	5.0
6	12 01 55.4	−18 52 49	109.0	4.1	1501	39	63.3
25	12 01 54.8	−18 52 49	3.5	1.6	1381	13	2.1
26	12 01 55.4	−18 52 49	1.4	1.8	1391	16	0.8
27	12 01 54.7	−18 52 49	1.4	1.4	1397	15	0.8
29	12 01 55.4	−18 52 48	6.1	1.9	1428	15	3.6
31	12 01 55.4	−18 52 48	3.6	2.0	1459	8	2.1
24	12 01 55.4	−18 52 48	1.5	2.0	1381	8	0.9
23	12 01 55.4	−18 52 47	8.3	2.3	1371	22	4.8
30	12 01 55.4	−18 52 47	2.2	2.0	1443	11	1.3
83	12 01 55.4	−18 52 47	1.4	1.8	1709	6	0.8
28	12 01 55.5	−18 52 46	3.4	2.0	1402	10	2.0
10	12 01 54.7	−18 52 44	14.9	2.8	1589	23	8.6
67	12 01 54.4	−18 52 44	5.7	1.8	1620	13	3.3
74	12 01 54.5	−18 52 44	0.6	1.4	1646	5	0.3
16	12 01 55.1	−18 52 41	16.0	2.5	1568	21	9.3
17	12 01 55.1	−18 52 40	11.4	3.1	1584	14	6.6
18	12 01 55.1	−18 52 38	7.3	2.9	1599	13	4.3
19	12 01 54.7	−18 52 34	23.6	2.2	1620	26	13.7
35	12 01 53.2	−18 52 33	0.6	1.5	1527	5	0.4
84	12 01 55.3	−18 52 33	1.9	1.8	1719	6	1.1
53	12 01 53.0	−18 52 32	1.6	1.7	1579	7	0.9
76	12 01 51.3	−18 52 31	2.1	2.5	1651	6	1.2
75	12 01 54.4	−18 52 30	2.0	1.4	1646	17	1.2
51	12 01 54.4	−18 52 29	9.2	1.6	1568	44	5.4
55	12 01 55.1	−18 52 29	4.7	2.1	1589	7	2.7
42	12 01 53.5	−18 52 28	0.8	1.4	1553	5	0.5
68	12 01 54.5	−18 52 28	3.5	1.5	1625	16	2.1
52	12 01 55.1	−18 52 26	2.2	1.9	1568	8	1.3
60	12 01 55.9	−18 52 25	1.7	2.4	1594	6	1.0
71	12 01 50.5	−18 52 24	16.5	1.9	1667	41	9.6
45	12 01 51.9	−18 52 22	0.7	1.6	1558	5	0.4
78	12 01 52.0	−18 52 20	4.1	1.6	1677	13	2.4
56	12 01 53.3	−18 52 16	2.1	1.4	1584	22	1.2
48	12 01 53.7	−18 52 12	1.3	1.4	1563	6	0.7
64	12 01 52.1	−18 52 08	4.7	1.3	1615	28	2.7
62	12 01 50.9	−18 52 07	5.4	1.6	1599	19	3.2
57	12 01 50.8	−18 52 06	2.4	1.4	1589	12	1.4
61	12 01 50.5	−18 52 06	0.6	1.5	1594	5	0.4
49	12 01 53.1	−18 52 05	1.5	1.6	1563	8	0.9
81	12 01 53.8	−18 52 04	1.7	1.4	1693	9	1.0
1	12 01 53.0	−18 52 02	152.4	6.7	1620	45	88.6
2	12 01 53.0	−18 52 01	50.8	5.8	1651	16	29.5
3	12 01 53.0	−18 52 01	35.9	4.5	1667	18	20.9
21	12 01 53.0	−18 52 00	19.5	2.4	1688	27	11.3

TABLE 2—*Continued*

ID[a]	α (J2000.0)	δ (J2000.0)	S_{CO} (Jy km s^{-1})	T_B[b] (K)	V_{lsr} (km s^{-1})	ΔV_{FWHM} (km s^{-1})	M_{mol} ($10^7 M_\odot$)
50.....	12 01 51.8	−18 51 58	1.2	1.3	1563	8	0.7
39.....	12 01 50.7	−18 51 57	9.1	1.7	1547	39	5.3
82.....	12 01 52.3	−18 51 57	4.7	1.5	1703	20	2.7
36.....	12 01 50.7	−18 51 54	7.1	1.5	1532	25	4.1
85.....	12 01 52.3	−18 51 54	1.9	1.6	1729	7	1.1
41.....	12 01 51.1	−18 51 52	17.2	2.1	1568	29	10.0
46.....	12 01 51.8	−18 51 41	4.5	2.3	1558	11	2.6
43.....	12 01 51.8	−18 51 38	4.9	2.5	1553	17	2.8

NOTES.—A distance to the Antennae of 19 Mpc is assumed throughout. Units of right ascension are hours, minutes, and seconds, and units of declination are degrees, arcminutes, and arcseconds.

[a] Cloud ID number assigned by CLFIND algorithm.

[b] Observed peak brightness temperature excess above the 2.74 K cosmic background.

[c] These clouds belong to the supergiant molecular complexes discussed in Paper I: complexes 4 and 5 in SGMC 2; complexes 7, 8, and 9 in SGMC 4; complex 15 in SGMC 5; complexes 22 and 58 in a part of NGC 4039.

APPENDIX B

CO-TO-H_2 CONVERSION FACTOR IN THE ANTENNAE

Most of the clouds identified in the Antennae are unresolved, so their masses can be calculated only from their CO flux. It is important, therefore, to estimate the CO-to-H_2 conversion factor that is appropriate for the Antennae by using the few clouds that are large enough that their true diameters can be deconvolved from the synthesized beam. We excluded clouds in the two galactic nuclei or near bright mid-infrared peaks from this analysis because the conversion factor could be modified in these regions because of intense star formation or high pressure (Bryant & Scoville 1996; Solomon et al. 1997).

We analyzed the data cube with CLFIND and CLSTATS by using three different contour levels (0.10, 0.11 = 2 σ, and 0.12 Jy beam^{-1}) as described above. The integrated intensity map for each cloud that appeared resolved in both dimensions from the output from CLSTATS was inspected to see whether it was in fact resolved. (Clouds may appear resolved from their sizes but not actually be resolved if, for example, the cloud is actually made up of two peaks or is highly elongated in one direction.) We identified four, three, and two clouds that appeared to be resolved when identified with contour levels of 0.10, 0.11, and 0.12 Jy beam^{-1}, respectively (Table 3). Only one cloud common to both the 0.10 and 0.11 Jy beam^{-1} processing was found. The remaining seven clouds were identified when contoured at different levels, but, because of small changes in how flux was assigned to each cloud, they did not always appear to be resolved spatially.

For each resolved cloud, the radius and velocity width were measured using CLSTATS, while the total CO flux was measured from a gain-corrected zeroth-moment map of each individual cloud. We used these measurements to calculate both the virial mass and the molecular mass. The virial mass is given by

$$M_{vir} = 198 \Delta V_{FWHM}^2 R_{pc}\ M_\odot\ ,$$

where ΔV_{FWHM} is the full-width half-maximum velocity in kilometers per second and $R_{pc} = (\mathrm{Area}/\pi)^{1/2}$ is the deconvolved

TABLE 3
RESOLVED CLOUDS USED TO DETERMINE X_{CO}

ID	S_{CO} (Jy km s^{-1})	R (pc)	ΔV_{FWHM} (km s^{-1})	M_{vir} ($10^8 M_\odot$)	M_{mol} ($10^8 M_\odot$)	CLFIND Contour (Jy beam^{-1})
17.....	28.6	580	33	1.3	1.7	0.12
39.....	9.6	430	23	0.45	0.56	0.12
19[a]	23.6	560	24	0.64	1.4	0.11
36.....	7.1	430	25	0.53	0.41	0.11
71.....	16.5	610	41	2.0	0.96	0.11
41.....	16.9	610	20	0.48	0.98	0.10
62.....	19.3	600	46	2.5	1.1	0.10
46.....	5.7	410	14	0.16	0.33	0.10

NOTES.—A distance to the Antennae of 19 Mpc is assumed throughout. Values for S_{CO} and ΔV_{FWHM} may differ from Table 2 for the clouds identified with a different contour level.

[a] This cloud was resolved for both the 0.11 and 0.10 Jy beam^{-1} contour levels. The values for all parameters are the average of two values.

TABLE 4
OTHER RESOLVED CLOUDS

ID	R (pc)	$\Delta V_{\rm FWHM}$ (km s^{-1})	$M_{\rm vir}$ ($10^8\ M_\odot$)	$M_{\rm mol}$ ($10^8\ M_\odot$)	ID from Paper I
1.....	760	45	3.1	8.9	NGC 4038
2.....	600	16	0.3	3.0	NGC 4038
3.....	630	18	0.4	2.1	NGC 4038
6.....	670	39	2.0	6.3	SGMC 1
12.....	670	53	3.7	2.4	SGMC 3
20.....	440	21	0.4	0.9	NGC 4039
21.....	480	27	0.7	1.1	NGC 4038

radius of the cloud in parsecs. The molecular mass is given by

$$M_{\rm mol} = 1.61 \times 10^4 D^2_{\rm Mpc} S_{\rm CO}\ M_\odot\ ,$$

where $D_{\rm Mpc}$ is the distance to the cloud in megaparsecs and $S_{\rm CO}$ is the CO integrated intensity in Jy km s^{-1} (Wilson & Scoville 1990). The ratio of the assumed value for CO-to-H_2 conversion factor in the Galaxy relative to the true value in the Antennae can then be determined from the ratio of the molecular mass to the virial mass. The average value of this ratio for the eight resolved clouds from the three different identification runs is 1.3 ± 0.3 with a standard deviation of 0.7. This result suggests that the CO-to-H_2 conversion factor may be slightly smaller in the Antennae than in the Milky Way. However, given that the ratio is consistent with equal conversion factors within the uncertainties, we have chosen to use the standard Galactic value [3×10^{20} H_2 cm^{-2} (K km s^{-1})$^{-1}$] for ease of comparison with other work.

Clouds that were resolved but were not used to determine the CO-to-H_2 conversion factor because of their location in the nuclei or the mid-infrared bright part of the overlap region are given in Table 4. Cross-identifications with Paper I are also given; note that in some cases several complexes in Table 2 and Table 4 correspond to a single supergiant molecular complex from Paper I. A comparison of the virial and molecular masses in Table 4 suggests that the CO-to-H_2 factor may be smaller than the adopted value in several of these clouds. In particular, the complexes in the nucleus of NGC 4038 all have molecular masses that exceed their virial masses by at least a factor of 3. This result suggests that the CO emission is overluminous in this galactic nucleus, perhaps similar to the effect seen in ultraluminous infrared galaxies (Solomon et al. 1997). We discuss the properties of the nuclear regions in a future paper (C. D. Wilson, S. C. Madden, & V. Charmandaris 2003, in preparation).

REFERENCES

Aalto, S., Hüttemeister, S., Scoville, N. Z., & Thaddeus, P. 1999, ApJ, 522, 165
Billett, O. H., Hunter, D. A., & Elmegreen, B. G. 2002, AJ, 123, 1454
Bryant, P. M., & Scoville, N. Z. 1996, ApJ, 457, 678
Casoli, F., Willaime, M.-C., Viallefond, F., & Gerin, M. 1999, A&A, 346, 663
Cen, R. 2001, ApJ, 560, 592
Cohen, R. S., Dame, T. M., Garay, G., Montani, J., Rubio, M., & Thaddeus, P. 1988, ApJ, 331, L95
Elmegreen, B. G. 1989, ApJ, 338, 178
Elmegreen, B. G., & Efremov, Y. N. 1997, ApJ, 480, 235
Evans, N. J., & Lada, E. A. 1991, in IAU Symp. 147, Fragmentation of Molecular Clouds and Star Formation, ed. E. Falgarone, F. Boulanger, & G. Duvert (Dordrecht: Kluwer), 293
Fabbiano, G., Krauss, M., Zezas, A., Rots, A., & Neff, S. 2003, ApJ, 598, 272
Fall, S. M., & Rees, M. J. 1985, ApJ, 298, 18
Fall, S. M., & Zhang, Q. 2001, ApJ, 561, 751
Feldmeier, J. J., Ciardullo, R., & Jacoby, G. H. 1997, ApJ, 479, 231
Ferrarese, L., et al. 1996, ApJ, 464, 568
———. 2000, ApJ, 529, 745
Gao, Y., Lo, K. Y., Lee, S.-W., & Lee, T.-H. 2001, ApJ, 548, 172
Garcia-Burillo, S., Guélin, M., & Cernicharo, J. 1993, A&A, 274, 123
Gelatt, A. E., Hunter, D. A., & Gallagher, J. S. 2001, PASP, 113, 142
Gibson, B. K., et al. 2000, ApJ, 529, 723
Harris, W. E. 2001, in Star Clusters, ed. L. Labhardt & B. Bingelli (Berlin: Springer), 223
Harris, W. E., & Pudritz, R. E. 1994, ApJ, 429, 177
Heyer, M. H., Carpenter, J. M., & Snell, R. L. 2001, ApJ, 551, 852
Hibbard, J. E., & Mihos, J. C. 1995, AJ, 110, 140
Hibbard, J. E., van der Hulst, J. M., Barnes, J. E., & Rich, R. M. 2001, AJ, 122, 2969
Ho, L. C., & Filippenko, A. V. 1996, ApJ, 466, L83
Holtzman, J. A., et al. 1992, AJ, 103, 691
Hunter, D. A., O'Connell, R. W., Gallagher, J. S., & Smecker-Hane, T. A. 2000, AJ, 120, 2383
Hunter, D. A., Shaya, E. J., Holtzman, J. A., Light, R. M., O'Neil, E. J., & Lynds, R. 1995, ApJ, 448, 179
Jog, C., & Solomon, P. M. 1992, ApJ, 387, 152
Johansson, L. E. B., et al. 1998, A&A, 331, 857
Johnstone, D., Wilson, C. D., Moriarty-Schieven, G., Joncas, G., Smith, G., Gregersen, E., & Fich, M. 2000, ApJ, 545, 327
Kennicutt, R. C., Jr. 1998, ApJ, 498, 541
Kramer, C., Stutzki, J., Röhrig, R., & Corneiussen, U. 1998, A&A, 329, 249
Kutner, M. L., et al. 1997, A&AS, 122, 255
Kwan, J. 1979, ApJ, 229, 567
Lada, E. A., Bally, J., & Stark, A. A. 1991a, ApJ, 368, 432
Lada, E. A., Evans, N. J., Depoy, D. L., & Gatley, I. 1991b, ApJ, 371, 171
Lamers, H. J. G. L. M., Panagia, N., Scuderi, S., Romaniello, M., Spaans, M., de Wit, W. J., & Kirshner, R. 2002, ApJ, 566, 818
Larsen, S. S. 2000, MNRAS, 319, 893
Larsen, S. S., & Richtler, T. 2000, A&A, 354, 836
Liang, M. C., Geballe, T. R., Lo, K. Y., & Kim, D.-C. 2001, ApJ, 549, L59
Massey, P., & Hunter, D. A. 1998, ApJ, 493, 180
McLaughlin, D. E., & Pudritz, R. E. 1996, ApJ, 457, 578
Mengel, S., Lehnert, M. D., Thatte, N., & Genzel, R. 2002, A&A, 383, 137
Mihos, J. C., Bothun, G. D., & Richstone, D. O. 1993, ApJ, 418, 82
Miller, B. W., Whitmore, B. C., Schweizer, F., & Fall, S. M. 1997, AJ, 114, 2381
Mirabel, I. F., et al. 1998, A&A, 333, L1
Motte, F., André, P., & Neri, R. 1998, A&A, 336, 150
Motte, F., André, P., Ward-Thompson, D., & Bontemps, S. 2001, A&A, 372, L41
Neff, S. G., & Ulvestad, J. S. 2000, AJ, 120, 670
O'Connell, R. W., Gallagher, J. S., Hunter, D. A., & Colley, W. N. 1995, ApJ, 446, L1
Planesas, P., Scoville, N., & Myers, S. T. 1991, ApJ, 369, 364
Rand, R. J. 1993, ApJ, 410, 68
———. 1995, AJ, 109, 2444
Rand, R. J., & Kulkarni, S. R. 1990, ApJ, 349, L43
Rand, R. J., Lord, S. D., & Higdon, J. L. 1999, ApJ, 513, 720
Rice, W., Lonsdale, C. J., Soifer, B. T., Neugebauer, G., Koplan, E. L., Lloyd, L. A., de Jong, T., & Habing, H. J. 1988, ApJS, 68, 91
Sakamoto, K. 1996, ApJ, 471, 173
Sakamoto, K., Scoville, N. Z., Yun, M. S., Crosas, M., Genzel, R., & Tacconi, L. J. 1999, ApJ, 514, 68
Salpeter, E. E. 1955, ApJ, 121, 161
Sanders, D. B., & Mirabel, I. F. 1985, ApJ, 298, L31
Sanders, D. B., Scoville, N. Z., & Solomon, P. M. 1985, ApJ, 289, 373

Sault, R. J., Teuben, P. J., & Wright, M. C. H. 1995, in ASP Conf. Ser. 77, Astronomical Data Analysis Software and Systems IV, ed. R. A. Shaw, H. E. Payne, & J. J. Hayes (San Francisco: ASP), 433
Schinnerer, E., Eckart, A., Tacconi, L. J., Genzel, R., & Downes, D. 2000, ApJ, 533, 850
Schweizer, F., Miller, B., Whitmore, B. C., & Fall, S. M. 1996, AJ, 112, 1839
Scoville, N. Z., Carlstrom, J. E., Chandler, C. J., Phillips, J. A., Scott, S. L., Tilanus, R. P. J., & Wang, Z. 1993, PASP, 105, 1482
Scoville, N. Z., Polletta, M., Ewald, S., Stolovy, S. R., Thompson, R., & Rieke, M. 2001, AJ, 122, 3017
Smith, L. J., & Gallagher, J. S. 2001, MNRAS, 326, 1027
Solomon, P. M., Downes, D., Radford, S. J. E., & Barrett, J. W. 1997, ApJ, 478, 144
Solomon, P. M., Rivolo, A. R., Barrett, J., & Yahil, A. 1987, ApJ, 319, 730
Stanford, S. A., Sargent, A. I., Sanders, D. B., & Scoville, N. Z. 1990, ApJ, 349, 492
Strong, A. W., et al. 1988, A&A, 207, 1
Testi, L., & Sargent, A. 1998, ApJ, 508, L91
Thornley, M. D., & Mundy, L. G. 1997, ApJ, 484, 202
Tully, R. B., & Fisher, J. R. 1988, Catalog of Nearby Galaxies (Cambridge: Cambridge Univ. Press)
Turner, A., et al. 1998, ApJ, 505, 207
Vigroux, L., et al. 1996, A&A, 315, L93
Whitmore, B. C. 2002, in IAU Symp. 207, Extragalactic Star Clusters, ed. D. Geisler, E. K. Grebel, & D. Minniti (San Francisco: ASP), 367
———. 2003, in A Decade of *Hubble Space Telescope* Science, ed. M. Livio, K. Noll, & M. Stiavelli (Cambridge: Cambridge Univ. Press), in press
Whitmore, B. C., & Schweizer, F. 1995, AJ, 109, 960
Whitmore, B. C., Schweizer, F., Leitherer, C., Borne, K., & Robert, C. 1993, AJ, 106, 1354
Whitmore, B. C., & Zhang, Q. 2002, AJ, 124, 1418
Whitmore, B. C., Zhang, Q., Leitherer, C., Fall, S. M., Schweizer, F., & Miller, B. W. 1999, AJ, 118, 1551
Williams, J. P., de Geus, E. J., & Blitz, L. 1994, ApJ, 428, 693
Wilson, C. D. 1995, ApJ, 448, L97
Wilson, C. D., & Scoville, N. Z. 1990, ApJ, 363, 435
Wilson, C. D., Scoville, N., Madden, S. C., & Charmandaris, V. 2000, ApJ, 542, 120 (Paper I)
Zhang, Q., & Fall, S. M. 1999, ApJ, 527, L81
Zhang, Q., Fall, S. M., & Whitmore, B. C. 2001, ApJ, 561, 727